

# Idea of thin-film beam splitters for two-colour beamlines

Hitoshi Abe\*

Institute of Materials Structure Science, High Energy Accelerator Research Organization, 1-1 Oho, Tsukuba, Ibaraki 305-0801, Japan, and Department of Materials Structure Science, School of High Energy Accelerator Science, SOKENDAI (The Graduate University for Advanced Studies), 1-1 Oho, Tsukuba, Ibaraki 305-0801, Japan. \*Correspondence e-mail: hitoshi.abe@kek.jp

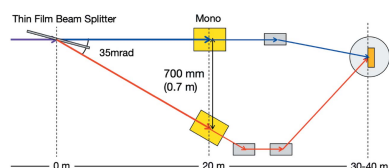
The idea to split soft X-ray and hard X-ray beams on the same axis into different directions is presented. A thin-film beam splitter can serve this purpose. Performances of thin-film beam splitters made of carbon and aluminium were examined. The idea of thin-film beam splitters expands possibilities in the design of two-colour beamlines.

## 1. Introduction

Synchrotron radiation science includes many scientific fields. Various experiments have been performed at synchrotron radiation facilities using a wide range of X-ray energies. Technically and habitually, we have two regions of X-rays: soft X-rays and hard X-rays. Soft X-rays have energies up to  $\sim 2$  keV, while hard X-rays have photon energies higher than  $\sim 2$  keV. X-rays in the 2–4 keV range are sometimes called tender X-rays. The 2 keV boundary between soft and hard X-rays is technically defined by the type of monochromator and the vacuum requirement conditions. Below 2 keV, grating monochromators are typically used and vacuum conditions are required. Above 2 keV, double-crystal monochromators made of Si are mostly used and measurements can be carried out under ambient conditions.

Moreover, properties that can be observed are essentially different for the two energy regions. Consider, for example, X-ray photoelectron spectroscopy (XPS) and X-ray absorption spectroscopy (XAS). XAS in the hard X-ray region is known as X-ray absorption fine-structure (XAFS) spectroscopy (Sayers *et al.*, 1971; Bunker, 2010; Evans, 2018). In the soft X-ray region, we can measure the 1s core electrons of organic elements such as C (284 eV), N (410 eV) and O (543 eV) (Stöhr, 1992). For the 3d transition metals, 2s and 2p electrons can be measured. Hard X-ray XAFS experiments give information on the electronic structures of unoccupied states (near-edge regions) and local atomic structures typically for 3d transition metals and heavier elements (Bunker, 2010; Evans, 2018).

Small-angle X-ray scattering (SAXS) and wide-angle X-ray scattering (WAXS) provide structural information over a wide length range (Bras *et al.*, 1993; Portale *et al.*, 2013; Shimizu *et al.*, 2013). Grazing-incidence SAXS (GISAXS) has attracted attention and GISAXS beamlines have recently been built (Hexemer *et al.*, 2010; Igarashi *et al.*, 2013). A combined method of SAXS and XAFS has also been reported (Nikitenko *et al.*, 2008; Bras *et al.*, 2010). In addition, there are a variety of experimental methods. Combinations of the



experimental methods mentioned above and others, and utilization of both soft and hard X-rays will produce new multi-modal experimental methods. Here, it should be noted that soft and hard X-rays each provide specific and unique information.

The same samples could be used at both soft and hard X-ray beamlines in order to understand their properties from various points of view. There are strong demands to use both soft and hard X-rays to measure the same samples under the same experimental conditions at the same place and same time. To understand catalytic chemical reactions, for example, both reacting molecules and catalysts should be observed. Reacting molecules, which usually contain C, N and O, should be observed by soft X-ray methods (Toyoshima *et al.*, 2012, 2014). Catalysts, which are typically 3d or heavier metal based materials, can be characterized by hard X-ray methods (Uemura *et al.*, 2011; Newton *et al.*, 2016; Abe *et al.*, 2017).

Beamlines where both soft and hard X-rays are available are strongly desired; let us call such beamlines two-colour beamlines hereafter. A two-colour beamline, beamline I09 (Lee & Duncan, 2018; Mudd *et al.*, 2014), is in operation at Diamond Light Source, Oxfordshire, UK. Beamline I09 has two insertion devices (IDs) for its light sources: one is a soft X-ray undulator and the other is a hard X-ray in-vacuum undulator. They are canted by 1.3 mrad, and the two beams are emitted in different directions. Each beam can be independently handled and delivered to the endstation at I09. Surface and bulk properties of V in  $\text{LiVOPO}_4$  have been reported (Wangoh *et al.*, 2016) by performing XPS for V 2p and XAFS for the V K-edge at beamline I09.

Beamline I09 is a clever design for building a two-colour beamline, but other ideas will be required to split a mixed beam from tandem coaxial IDs into soft X-rays and hard X-rays. A set of tandem coaxial IDs would fit extremely low emittance synchrotron radiation rings. A beam splitter for such a mixed coaxial beam will help in the design of two-colour beamlines.

In this paper, the idea of beam splitters to split a mixed coaxial beam into soft X-ray and hard X-ray beams is presented. Thin films can be used to split the beam of soft and hard X-rays: these are called thin-film beam splitters (TFBSs). TFBSs expand the possible optical layouts for designing two-colour beamlines.

## 2. Method

The reflectivity for soft X-rays of 200–2000 eV and transmission for hard X-rays of 2–20 keV were calculated to examine the feasibility of TFBSs. TFBSs can split a mixed beam of soft and hard X-rays into two beams, as shown in Fig. 1: one beam consists of soft X-rays reflected at the surface of the TFBS, and the other consists of hard X-rays passing through the TFBS. X-ray interaction properties (Henke *et al.*, 1993; Hubbell *et al.*, 1975), which are available from the database of the Center for X-Ray Optics (CXRO; Berkeley, California, USA), were used for these calculations. Two elements, carbon and aluminium, were selected as the materials for the TFBSs. Several incident

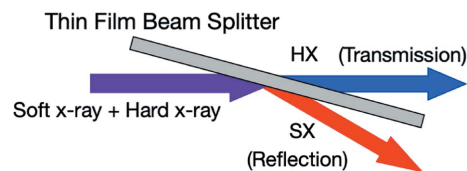


Figure 1

Schematic concept of TFBS. Soft X-rays (SX) are reflected at the surface of the TFBS, and hard X-rays (HX) pass through it. TFBSs can split a mixed beam of soft and hard X-rays into two beams.

angles were simulated for the reflectivity calculations. The thickness dependence of the transmission was examined.

## 3. Results and discussion

The feasibility of TFBSs is examined. TFBSs should show high reflectivity in the soft X-ray region and high transmission for hard X-rays. The reflectivity strongly depends on the angle of the incident radiation, and the high transmission requires light elements for the materials of TFBSs. TFBSs made of lighter elements placed at smaller incident angles will work better. Here, TFBSs made of two different elements, carbon and aluminium, were studied.

### 3.1. TFBS made of carbon

The reflectivity of soft X-rays by a carbon TFBS is shown in Fig. 2. The dot-dashed, dashed, dotted and solid lines denote the incident angles of 3, 2, 1.5 and 1°, respectively. The sharp dip at 280 eV is due to the absorption by carbon, and we will discuss the usability of soft X-rays from ~300 eV up to 2000 eV.

An incident angle of 3° reflects less than 50% of the incoming X-rays over the whole soft X-ray range considered here. A reflectivity of less than 50% is useless for our purposes because it is weaker than the way which geometrically splits a beam into two beams. The smaller the angle becomes, the stronger and wider the reflectivity increases. At an incident angle of 1°, more than 70% of the incoming X-rays from ~300 to 1730 eV are reflected. Therefore it is useful if carbon TFBSs

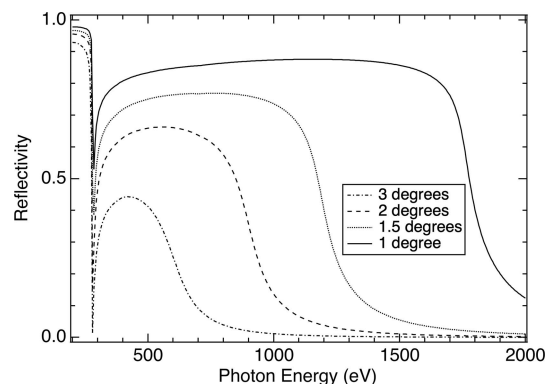


Figure 2

Reflectivity of soft X-rays by a carbon TFBS. The dot-dashed, dashed, dotted and solid lines denote incident angles of 3, 2, 1.5 and 1°, respectively. The sharp dip at 280 eV is due to absorption by carbon.

**Table 1**  
Angle  $\alpha$  and related values.

$\alpha$ ( $^\circ$ )	$\sin \alpha$	$1/\sin \alpha$	$\sim 1/\sin \alpha$
1	0.01745	57.298	60
2	0.03489	28.653	30
3	0.05233	19.107	20
6	0.10452	9.567	10

are placed at incident angles of  $1^\circ$  for soft X-ray measurements in this energy range.

A carbon TFBS should transmit hard X-rays if it is to work as a beam splitter. The transmission of hard X-rays through a carbon TFBS has been examined. Consider X-rays passing through a carbon TFBS with an effective length  $L$ , which is the thickness  $t$  divided by the sine of the incident angle  $\alpha$ , *i.e.*  $L = t/\sin \alpha$ ; thus the effective length  $L$  depends on both the TFBS thickness  $t$  and the X-ray incident angle  $\alpha$ . When angle  $\alpha$  is  $1^\circ$ ,  $1/\sin \alpha = 57.298 \approx 60$ , and  $L = t \times 60$ . Values for angle  $\alpha$ ,  $\sin \alpha$  and  $1/\sin \alpha$  are summarized in Table 1. An effective length  $L$  of  $\sim 600 \mu\text{m}$  corresponds to a  $10 \mu\text{m}$ -thick carbon TFBS placed at  $\alpha = 1^\circ$  or a  $20 \mu\text{m}$ -thick carbon TFBS placed at  $\alpha = 2^\circ$ , for instance.

Let us consider placing a carbon TFBS at an X-ray incident angle  $\alpha = 1^\circ$ , where the reflectivity of the soft X-ray range is useful. The transmission of hard X-rays is shown in Fig. 3 for different effective lengths  $L$ , from  $L = 600 \mu\text{m}$  down to  $L = 12 \mu\text{m}$ . Less than 50% of incoming X-rays below  $\sim 7.5 \text{ keV}$  can pass through the the TFBS with  $L = 600 \mu\text{m}$ . This is not useful, so we would like to use thinner TFBSs, *i.e.* those with smaller values of  $L$ . The TFBSs with  $L = 300, 120, 60, 30$  and  $12 \mu\text{m}$  give  $\sim 6, 4.5, 3.6, 2.9$  and  $2.1 \text{ keV}$  as the onset of 50% transmission, respectively. Thinner TFBSs are better, but a TFBS with  $L = 60 \mu\text{m}$ , *i.e.* a carbon TFBS of thickness  $t = 1 \mu\text{m}$  placed at  $\alpha = 1^\circ$ , enables 50% transmission above  $\sim 3.6 \text{ keV}$  and 70% transmission above  $\sim 4.5 \text{ keV}$ . More than 90% of incoming X-rays are available above  $\sim 6.6 \text{ keV}$ , which can be regarded as almost transparent for this energy region.

### 3.2. TFBS made of aluminium

The reflectivity of soft X-rays by an Al TFBS is shown in Fig. 4. The dot-dashed, dashed, dotted and solid lines represent the reflectivity at incident angles of  $3, 2, 1.5$  and  $1^\circ$ , respectively. The sharp dip at  $\sim 1560 \text{ eV}$  is due to the absorption by aluminium. An incident angle  $\alpha = 3^\circ$  reflects only the range  $\sim 200\text{--}560 \text{ eV}$  with the 50% criterion of the incoming flux. The upper limit of the energy range for the 50% criterion increases to  $\sim 1530 \text{ eV}$  with decreasing incident angle down to  $1^\circ$ .

The transmission of hard X-rays through an Al TFBS is shown in Fig. 5. The same discussion as for the carbon TFBS is applied, and effective lengths  $L$  of  $600, 300, 120, 60, 30, 12, 6$  and  $3 \mu\text{m}$  were examined. When the incident angle is set at  $\alpha = 1^\circ$ , these  $L$  values correspond to actual thicknesses  $t$  of  $10, 5, 2, 1, 0.5, 0.2, 0.1$  and  $0.05 \mu\text{m}$ , respectively. TFBSs with  $L = 600$  and  $300 \mu\text{m}$  are useless because only X-rays above  $\sim 15 \text{ keV}$  can pass through with 50% criterion. Thinner ones provide

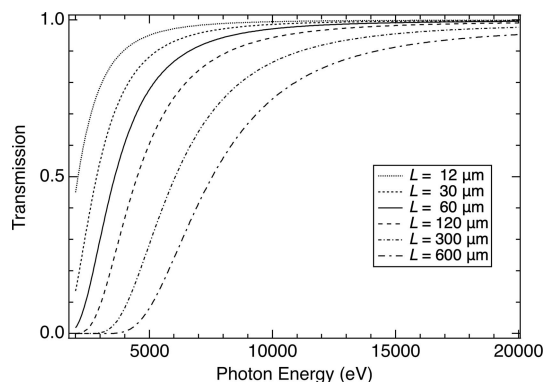


**Figure 3**  
Transmission of soft X-rays through a carbon TFBS. Each line denotes a certain effective length  $L$  as indicated in the legend.

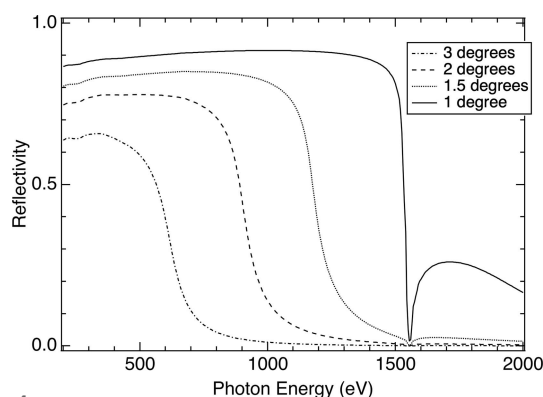


**Figure 4**  
Reflectivity of soft X-rays by an aluminium TFBS. The dot-dashed, dashed, dotted and solid lines denote incident angles of  $3, 2, 1.5$  and  $1^\circ$ , respectively. The sharp dip at  $\sim 1560 \text{ eV}$  is due to absorption by aluminium.

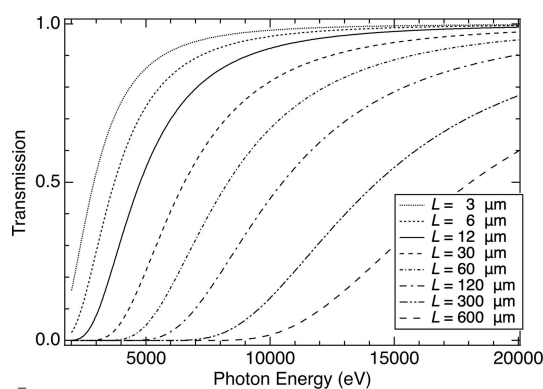


**Figure 5**  
Transmissions of hard X-rays through the aluminium TFBS. Each line denotes a certain effective length  $L$  as indicated in the legend.

X-rays of lower energy range. The energy range provided by a TFBS with  $L = 30 \mu\text{m}$  is above  $6.5 \text{ keV}$  by the 50% criterion. This condition is somewhat useful. If it is possible to prepare a thin film with  $L = 12 \mu\text{m}$  ( $t = 0.2 \mu\text{m}$ ), we can use hard X-rays above  $\sim 4.8 \text{ keV}$  with the 50% criterion.

### 3.3. TFBS and two-colour beamline layouts

Fig. 6 summarizes the performances of carbon and aluminium TFBSs over the whole energy range discussed here.

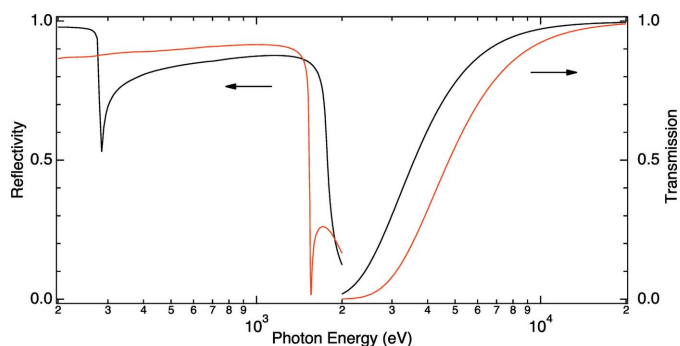


**Figure 6**  
TFBS performances of carbon (black line) and aluminium (red line) from 200 eV to 20 keV. These are the 1  $\mu\text{m}$  carbon TFBS ( $L = 60 \mu\text{m}$ ) and the 0.2  $\mu\text{m}$  Al TFBS ( $L = 12 \mu\text{m}$ ) both placed at  $\alpha = 1^\circ$ .

Curves are plotted for a  $t = 1 \mu\text{m}$  carbon TFBS placed at  $\alpha = 1^\circ$  and a  $t = 0.2 \mu\text{m}$  Al TFBS placed at  $\alpha = 1^\circ$ . Using the carbon TFBS, soft X-rays up to  $\sim 1780 \text{ eV}$  and hard X-rays above 3.6 keV are available with the 50% criterion of the incoming flux. Even with the 70% criterion, we can use soft X-rays of  $\sim 300\text{--}1730 \text{ eV}$  and hard X-rays above  $\sim 4.5 \text{ keV}$ . The Al TFBS provides soft X-rays up to  $\sim 1530 \text{ eV}$  and hard X-rays above 4.8 keV with the 50% criterion of the incoming flux. The 70% criterion gives us soft X-rays up to  $\sim 1520 \text{ eV}$  and hard X-rays above  $\sim 6 \text{ keV}$ .

Thus, TFBSs made of carbon and aluminium have great potential to be used as beam splitters for building two-colour beamlines. The reflectivity of aluminium TFBSs is higher than that of carbon ones in the soft X-ray range. For the hard X-ray range, carbon TFBSs provides more flux than the aluminium ones. A downside of the carbon TFBS is the dip by the absorption of the carbon *K*-edge at 280 eV. Drawbacks of the Al TFBS are the dip by the absorption of the Al *K*-edge at  $\sim 1560 \text{ eV}$  and the relatively low transmission of hard X-rays compared with the carbon ones. We would like to avoid the dip at 280 eV for carbon measurements, and also higher transmission for the hard X-ray range is desired. One solution is to fabricate an Al-coated carbon TFBS. A surface Al layer will exhibit a similar reflectivity as the red line shown in Fig. 6 up to 2000 eV, and a similar transmission as the black line above 2000 eV will be provided because the main body is made of carbon. An Al-coated carbon TFBS will have the best of both ranges.

Finally, possible layouts of monochromators and beamline optics are suggested. When a TFBS is placed at an incident angle  $\alpha = 1^\circ$ , the splitting angle between soft X-rays and hard X-rays is  $2^\circ$ , which is  $\sim 35 \text{ mrad}$ . Two mono-

chromators, one for soft X-rays and the other for hard X-rays, can be installed at 20 m from the TFBS with a separation distance of 0.7 m as shown in Fig. 7(a). The two beams will be independently handled and can be focused at the same position. Variations of layouts are schematically depicted in Fig. 7(b). Fig. 7(b-1) shows a two-colour use in the literal sense. The two beams are focused at the same point at the same time. Parallel-use and connected-use layouts are presented in Figs. 7(b-2) and 7(b-3). These layouts provide opportunities to carry out two measurements at the same time. Two-colour beamlines of these types can accept two different groups at the same time.

Two issues that need to be overcome should be mentioned in order to use TFBSs in two-colour beamlines: one is the fabrication of uniform thin films of a certain size, and the other is the heat load from the incoming X-rays. The former will become easier when small-sized beams are available at new or next-generation light sources. When a beam is incident on a TFBS at an incident angle of  $1^\circ$ , its footprint on the TFBS becomes  $\sim 60$  times larger than the beam size. A beam size of 1 mm yields a  $\sim 60 \text{ mm}$  footprint, and thus a TFBS larger than 60 mm would need to be installed and kept stably flat. It would be difficult to meet this condition, but a far smaller beam should allow us this possibility. If the beam size becomes smaller, down to  $\sim 10 \mu\text{m}$ , a TFBS smaller than 1 mm can be used. Actually, a 150 nm-thick Ni thin film, whose diameter is larger than 3 mm, has already been installed and used at a slow

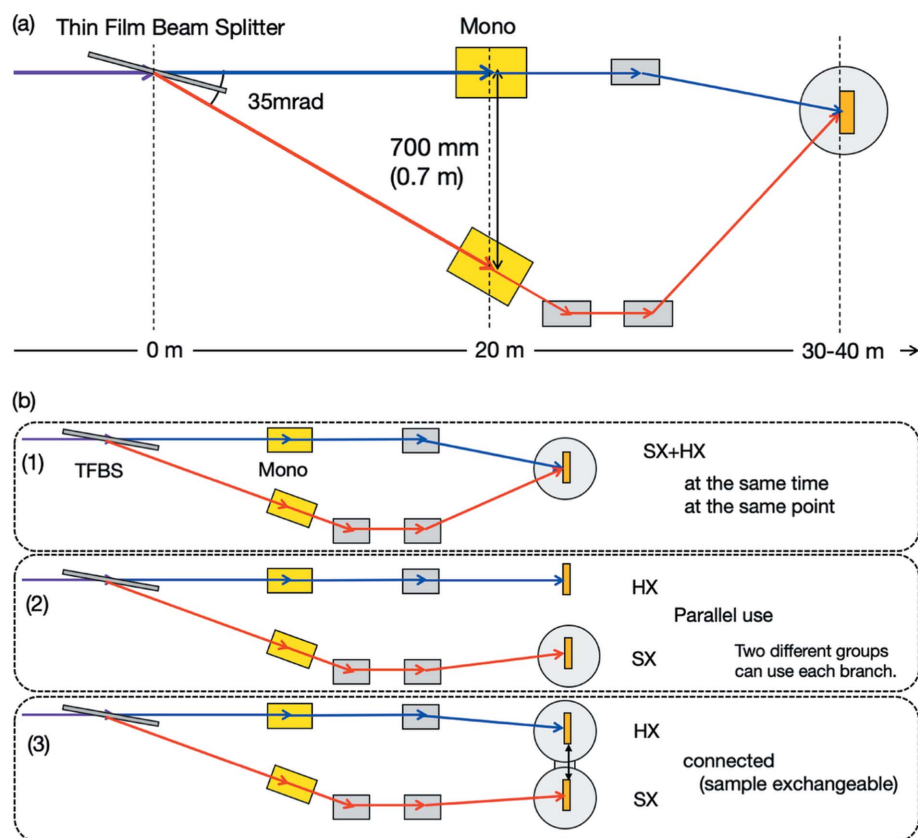


**Figure 7**  
(a) Possible layout of a TFBS and two monochromators. (b) Variations of two-colour beamlines.

positron facility (Fujinami *et al.*, 2008; Wada *et al.*, 2018). The fabrication of such thin films has a long history (Zafar *et al.*, 1988, 1989), and it will become possible to prepare suitable films for TFBSs in the near future. The latter issue, the heat load issue, would be serious but cryogenic nitrogen can be used to handle such heat loads. Further ways to overcome the heat load issue are expected in the future.

#### 4. Summary

The idea of using thin-film beam splitters to split soft X-ray and hard X-ray beams in the same axis has been presented. The performances of TFBSs made of carbon and aluminium were examined. TFBSs are useful for building two-colour beamlines, where soft X-ray and hard X-ray measurements can be performed for the same sample at the same time.

#### Acknowledgements

The author is grateful to Professor Iwao Matsuda at the University of Tokyo for fruitful discussions.

#### References

Abe, H., Niwa, Y., Kitano, M., Inoue, Y., Sasase, M., Nakao, T., Tada, T., Yokoyama, T., Hara, M. & Hosono, H. (2017). *J. Phys. Chem. C*, **121**, 20900–20904.

Bras, W., Derbyshire, G., Ryan, A., Mant, G., Felton, A., Lewis, R., Hall, C. & Greaves, G. (1993). *Nucl. Instrum. Methods Phys. Res. A*, **326**, 587–591.

Bras, W., Nikitenko, S., Portale, G., Beale, A., Eerden, A. & Detollenaere, D. (2010). *J. Phys. Conf. Ser.* **247**, 012047.

Bunker, G. (2010). *Introduction to XAFS: A Practical Guide to X-ray Absorption Fine Structure Spectroscopy*. Cambridge University Press.

Evans, J. (2018). *X-ray Absorption Spectroscopy for the Chemical and Materials Sciences*. Wiley.

Fujinami, M., Jinno, S., Fukuzumi, M., Kawaguchi, T., Oguma, K. & Akahane, T. (2008). *Anal. Sci.* **24**, 73–79.

Henke, B. L., Gullikson, E. M. & Davis, J. C. (1993). *At. Data Nucl. Data Tables*, **54**, 181–342.

Hexemer, A., Bras, W., Glossinger, J., Schaible, E., Gann, E., Kirian, R., MacDowell, A., Church, M., Rude, B. & Padmore, H. (2010). *J. Phys. Conf. Ser.* **247**, 012007.

Hubbell, J. H., Veigele, W. J., Briggs, E. A., Brown, R. T., Cromer, D. T. & Howerton, R. J. (1975). *J. Phys. Chem. Ref. Data*, **4**, 471–538.

Igarashi, N., Shimizu, N., Koyama, A., Mori, T., Ohta, H., Niwa, Y., Nitani, H., Abe, H., Nomura, M., Shioya, T., Tsuchiya, K. & Ito, K. (2013). *J. Phys. Conf. Ser.* **425**, 072016.

Lee, T.-L. & Duncan, D. A. (2018). *Synchrotron Radiat. News*, **31**(4), 16–22.

Mudd, J. J., Lee, T.-L., Muñoz-Sanjosé, V., Zúñiga-Pérez, J., Payne, D. J., Egdell, R. G. & McConville, C. F. (2014). *Phys. Rev. B*, **89**, 165305.

Newton, M. A., Brazier, J. B., Barreiro, E. M., Parry, S., Emmerich, H., Adrio, L. A., Mulligan, C. J., Hellgardt, K. & Hii, K.-K. (2016). *Green Chem.* **18**, 406–411.

Nikitenko, S., Beale, A. M., van der Eerden, A. M. J., Jacques, S. D. M., Leynaud, O., O'Brien, M. G., Detollenaere, D., Kaptein, R., Weckhuysen, B. M. & Bras, W. (2008). *J. Synchrotron Rad.* **15**, 632–640.

Portale, G., Cavallo, D., Alfonso, G. C., Hermida-Merino, D., van Drongelen, M., Balzano, L., Peters, G. W. M., Goossens, J. G. P. & Bras, W. (2013). *J. Appl. Cryst.* **46**, 1681–1689.

Sayers, D. E., Stern, E. A. & Lytle, F. W. (1971). *Phys. Rev. Lett.* **27**, 1204–1207.

Shimizu, N., Mori, T., Igarashi, N., Ohta, H., Nagatani, Y., Kosuge, T. & Ito, K. (2013). *J. Phys. Conf. Ser.* **425**, 202008.

Stöhr, J. (1992). *NEXAFS Spectroscopy*. Springer-Verlag Berlin Heidelberg.

Toyoshima, R., Yoshida, M., Monya, Y., Kousa, Y., Suzuki, K., Abe, H., Mun, B.-S., Mase, K., Amemiya, K. & Kondoh, H. (2012). *J. Phys. Chem. C*, **116**, 18691–18697.

Toyoshima, R., Yoshida, M., Monya, Y., Suzuki, K., Amemiya, K., Mase, K., Mun, B.-S. & Kondoh, H. (2014). *Phys. Chem. Chem. Phys.* **16**, 23564–23567.

Uemura, Y., Inada, Y., Bando, K. K., Sasaki, T., Kamiuchi, N., Eguchi, K., Yagishita, A., Nomura, M., Tada, M. & Iwasawa, Y. (2011). *J. Phys. Chem. C*, **115**, 5823–5833.

Wada, K., Shirasawa, T., Mochizuki, I., Fujinami, M., Takahashi, T., Maekawa, M., Kawasuso, A., Kimura, M. & Hyodo, T. (2018). *JJAP Conf. Proc.* **7**, 011301.

Wangoh, L. W., Sallis, S., Wiaderek, K. M., Lin, Y.-C., Wen, B., Quackenbush, N. F., Chernova, N. A., Guo, J., Ma, L., Wu, T., Lee, T.-L., Schlueter, C., Ong, S. P., Chapman, K. W., Whittingham, M. S. & Piper, L. F. J. (2016). *Appl. Phys. Lett.* **109**, 053904.

Zafar, N., Chevallier, J., Jacobsen, F. M., Charlton, M. & Laricchia, G. (1988). *Appl. Phys. A*, **47**, 409–412.

Zafar, N., Chevallier, J., Laricchia, G. & Charlton, M. (1989). *J. Phys. D Appl. Phys.* **22**, 868–870.